Moho topography beneath the Eastern European Alps by global phase seismic interferometry

Irene Bianchi[1,2], Elmer Ruigrok[3,4], Anne Obermann[5], and Edi Kissling[5]

[1]Istituto Nazionale di Geofisica e Vulcanologia, Via di Vigna Murata 605, 00143, Rome, Italy
[2]Institut für Meteorologie und Geophysik, Universität Wien, 1090 Wien Althanstraße 14 (UZA II)
[3]Royal Netherlands Meteorological Institute, De Bilt, The Netherlands
[4]Utrecht University, Utrecht, The Netherlands
[5]Swiss Seismological Service, ETH Zurich, Zurich, Switzerland

Correspondence: Irene Bianchi (irene.bianchi@univie.ac.at)

Abstract. In this work we present the application of the Global-Phase Seismic Interferometry (GloPSI) technique to a data-set recorded across the Eastern Alps with the EASI temporary seismic network (Eastern Alpine Seismic Investigation). GloPSI aims at rendering an image of the lithosphere from the waves that travel across the core before reaching the seismic stations (i.e. PKP, PKiKP, PKIKP). The technique is based on the principle that a stack of autocorrelations of transmission responses mimics the reflection response of a medium, and is used here to retrieve information about the crust-mantle boundary, such as its depth and topography. We produce images of the upper lithosphere using 64 teleseismic events. We notice that with GloPSI, we can well image the topography of the Moho in regions where it shows a nearly planar behaviour (i.e. in the northern part of the profile, from the Bohemian massif to beneath the Northern Calcareous Alps). Below the higher crests of the Alpine chain, and the Tauern Window in particular, we cannot find evidence for a typical boundary between crust and mantle. The GloPSI results indicate the absence of an Adriatic crust made of laterally continuous layers smoothly descending southwards. Our results confirm the observations of previous studies suggesting a structurally complex and faulted internal Alpine crustal structure.

1 Introduction

As part of the Alpine-Himalayan orogen, the European Alps are the result of the subduction of the Alpine Tethys and European paleomargin beneath the Adriatic microplate and the subsequent continent-continent collision that led to a 200 km wide convergence zone with a significant crustal root (e.g. Handy et al., 2015, and references therein). After the closure of major and minor oceans, the Alpine Tethys with its several arms and embayments such as the Penninic and the Meliata oceans (e.g. Neubauer et al., 2000), the continental Europe and continental parts of the much smaller plate Adria collided (e.g Handy et al., 2010). For the Eastern Alps, tectonic reconstructions have shown that the convergence between the two plates involved hundreds of kilometres, though there is no consensus on the precise amount of shortening (Rosenberg et al., 2018, and references therein). Likewise, while there is a general agreement that the European and the Adriatic Moho are offset across the plate boundary in the Alps, the exact Moho topography beneath the Eastern Alps is still a matter of debate.

With nearly 200 controlled source seismic (CSS) profiles in the greater Alpine region (e.g., Roure et al., 1990; Blundell et al., 1992; Scarascia and Cassinis, 1997; Fantoni et al., 2003; Kissling et al., 2006; Brückl et al., 2007; Hrubcova and Geissler, 2009; Grad et al., 2009), arguably the Alps denote the best studied orogen by both refraction and near-vertical reflection seismics. In near-vertical reflection seismic profiles along several transects across the Alps (Roure et al., 1990; Pfiffner et al., 1997; TRANSALP Working Group et al., 2002), the Moho has been commonly imaged as a relatively narrow band of high reflectivity (e.g. Holliger and Kissling, 1991), and along the TRANSALP transect this high reflectivity Moho band well correlates with the results obtained by receiver functions (Kummerow et al., 2004). Several long-range seismic experiments have been carried out in the Eastern Alpine area, like the Alpine longitudinal profile (named ALP75) extended along the axis of the Western and Eastern Alps, reaching the Pannonian basin (Yan and Mechie, 1989; Scarascia and Cassinis, 1997); the Cel09 profile crossing the Bohemia massif (Hrubcová et al., 2005), and the long range CSS experiments, named CELEBRATION 2000 and ALP 2002, that covered the area from the Eastern European platform in the north-east to the Adriatic foreland in the south-west (Guterch et al., 2004; Brückl et al., 2003). The temporary dense deployment of passive seismic stations within the EASI project (Eastern Alpine Seismic Investigation, AlpArray Working Group, 2014; Hetényi et al., 2018) was conceived to add information on the crustal structure and Moho depth, with respect to previous investigations through a set of high-quality seismic data. The temporary EASI array consisted of 55 broadband seismic stations deployed along a 550 km north-south transect from the Bohemian Massif to the Adriatic coast at a Longitude of about 13.4°E (Figure 1). EASI followed the same trajectory as one of the ALP 2002 profiles, namely the Alp01 (Brückl et al., 2007), which extended from the Bohemian Massif to the Adriatic foreland (Figure 1). The trajectory of EASI crosses the lines of two of the previously mentioned active seismic profiles, namely the Cel09 (Hrubcová et al., 2005; Hrubcova and Geissler, 2009) and ALP75 (Yan and Mechie, 1989). Both show the Moho depth with low uncertainties. EASI, at 110 km from its northern edge, crosses the Cel09, according to which the European Moho interface is at 32 km depth; at 375 km from its northern edge, EASI crosses ALP75, which marks the European Moho at 48 km depth.

Most of the information we have about the Moho in the study area are derived from CSS experiments (e.g. Yan and Mechie, 1989; Scarascia and Cassinis, 1997; Waldhauser et al., 2002; Bleibinhaus and Gebrande, 2006; Behm et al., 2007; Brückl et al., 2007; Diehl et al., 2009; Hrubcova and Geissler, 2009; Spada et al., 2013). The CSS profiles provide reliable but very sparse information about the Moho topography that needs to be interpolated and is interpreted with a Moho triple junction (Brückl et al., 2007) or with a Moho gap (Bleibinhaus and Gebrande, 2006) (see Figure 1). The latter interpretation is strongly supported by Spada et al. (2013) based on critically assessing all available seismic information about the Moho beneath the Alps with regards to their reliability, 3D migration and depth uncertainties and considering the results of PmP mapping presented by Bleibinhaus and Brückl (2006) and Behm et al. (2007). Several attempts were made to image the Moho discontinuity in the Eastern Alps with passive seismic methods exploiting distant earthquakes. Single station~~s~~ receiver function analysis by both Ps and Sp (Bianchi et al., 2014, 2015) gave scattered values when locating the Moho beneath the higher Alpine crests, suggesting the presence of several seismic discontinuities and anisotropy (Bianchi and Bokelmann, 2014). The interpretation of the receiver function (RF) data set along EASI (Hetényi et al., 2018) shows a clear difference between the signal in the northern part of the profile, where the European Moho is clearly imaged by different approaches, and the southern part of the profile,

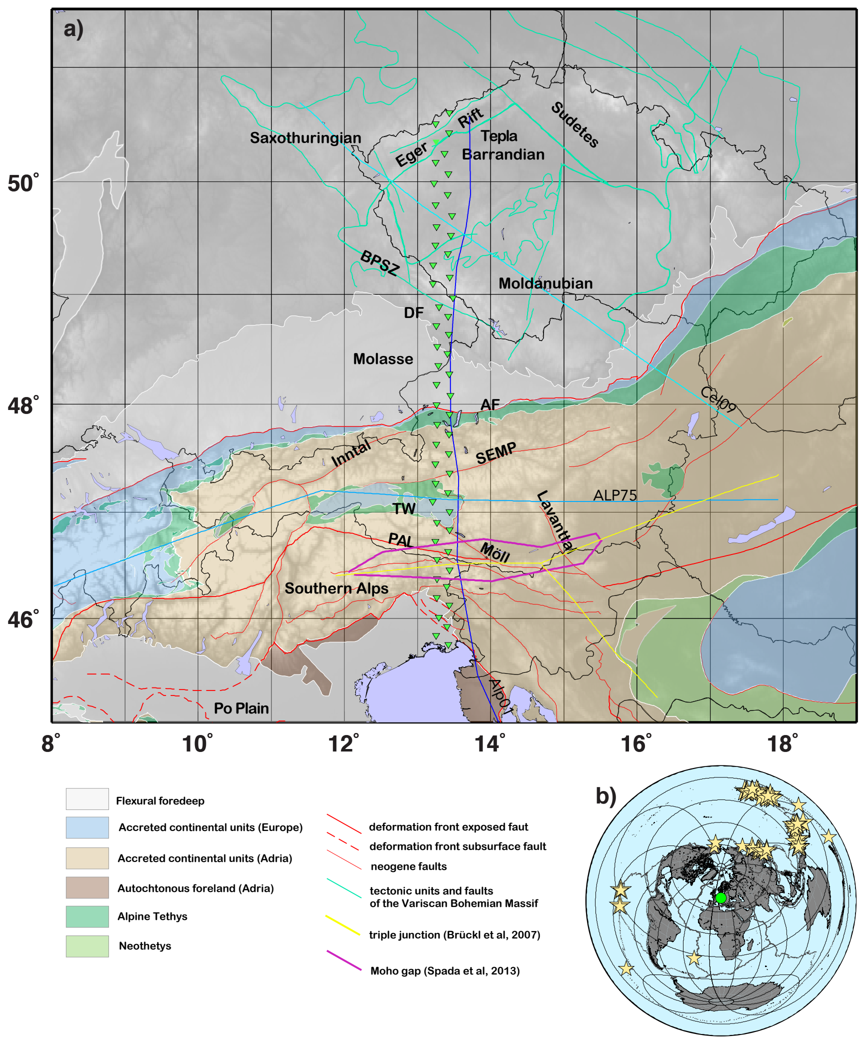

Figure 1. a) Map of the wider study area showing the location of the seismic stations (green triangles) and the traces of previous active seismic profiles (ALP75, Cel09, Alp01). Colours on the background correspond to the generalized tectonic map of the Alps (Bigi et al., 1990; Bousquet et al., 2012; Froitzheim et al., 1996; Handy et al., 2010; Schmid et al., 2004, 2008). b) Globe with the location of EASI transect (green) and epicenters of teleseisms used for GloPSI imaging (stars). Relief model of Earth's surface used is ETOPO1 (NOAA National Geophysical Data Center, Accessed: 2019; Amante and Eakins, 2009).

where the RF results show several features of limited extent and at depth intervals that may correspond to either the lower crust and/or the mantle lithosphere. Near the southern end of the EASI profile, the RF results image the Adria Moho dipping slightly towards north. In conclusion, in the wide central section of the Eastern Alps the Moho is not well imaged due to poorly reflective signals (PmP phases from CSS, e.g. Bleibinhaus and Gebrande, 2006; Behm et al., 2007) or weak converted signals by RF (Hetényi et al., 2018). Recent ambient noise tomography studies attempt to infer estimates on the Moho topography in the area (Sadeghi-Bagherabadi et al., submitted; Qorbani et al., 2020; Molinari et al., 2020; Lu et al., 2020), the used technique is rather valuable for identifying lateral velocity variation, and the results are showing the high variability of the crustal structures. Here, we use seismic interferometry applied to the records of distant earthquakes, for adding information on the long-debated nature of the lower crust and Moho in this part of the Eastern Alps. The term seismic interferometry refers to the principle of generating new seismic responses of virtual sources (Schuster, 2001) by correlating seismic observations at different receiver locations. We estimate lithospheric-scale reflection responses by autocorrelating and stacking primarily global phases; waves that travel across the core before reaching the seismic stations. Through autocorrelation, a response is obtained that would be measured if there was a co-located source and receiver at the same station. This novel technique has been developed and presented in Ruigrok and Wapenaar (2012), and in the last years was applied for several case studies for imaging the Earth's lithosphere (Nishitsuji et al., 2016; Frank et al., 2014; Van Ijsseldijk et al., 2019). With the aforementioned implementations, reflectors are well imaged when they are illuminated with angles of incidence close to zero. RFs on the other hand, only show signals when the angle of incidence is considerably greater than zero. This complementary nature of both techniques gives the promise that additional information on the Alpine reflectively can be found with seismic interferometry. In other implementations with distant seismicity, primarily P-phase correlations are used (Ruigrok et al., 2010; Sun and Kennett, 2016; Pham and Tkalcic, 2017; Tauzin et al., 2019). Based on results from previous applications, we expect that this technique helps identifying the Moho as the boundary between a reflective crust and a less reflective mantle.

2 DATA and METHOD

2.1 DATA

We collected broadband data from 55 seismic stations belonging to the EASI transect (fully operating between 08/2014 and 08/2015, see Hetényi et al., 2018), now publicly available through EIDA website (https://www.orfeus-eu.org/). We selected earthquakes within the recording time of the EASI deployment at epicentral distances (Δ) between 120° and 180° with M> 5.6. To increase the ray-parameter range, we added events from the northern and southern backazimuthal directions between 70° and 90° Δ, to give an in-line illumination of the profile. After visual inspection, we retain a total of 64 events with high SNR around the P onset (listed in Table T1). We have used PKIKP phases (events from Δ larger than 120°) which arrive subvertically below the seismic stations and are added to this a handful of P- phases from epicentral distances 70°-90°, to improve the imaging of dipping structure. We discarded events occurring around 150° Δ, for which we observe triplications of the P wave (Adams and Randall, 1963) (i.e. we discarded the time windows with multiple dominant phase responses). The selected 64 events display a high station coverage. Our study makes use of the records starting at 10s before and ending 80s after the onset of the P-wave. This time window contains most of the source-side and receiver side scattering.

2.2 METHOD

For the computation of the GloPSI images, we largely follow the steps indicated in Ruigrok and Wapenaar (2012). Below we are succint on steps that are identical and give more explanation on updated processing. The P-direct waves reaching the single seismic station are followed by reverberations that reflect at seismic interfaces at depth and reach the receiver again. Following Claerbout (1968) and Wapenaar (2003) the reflection response at the seismic station is achieved by autocorrelating the transmission response, selecting minus the causal result and muting the delta pulse. We repeat the autocorrelation step for varying illumination angles and for varying source depths. Then we stack together the results in order to enhance signals with the correct timing (Snieder, 2004) and to suppress spurious cross terms due to depth phases (Ruigrok et al., 2010). For the phases used, the ray parameter varies from 0 to 0.06 s/km, which suffices to retrieve the zero-offset response (i.e. coinciding source and receiver at the surface) for horizontal and gently dipping interfaces. In the following we list the various processing steps to end up with an estimate of the primary-only zero-offset reflection response at each EASI station.

- After applying instrument-response deconvolution and bandpass filtering (0.04 to 0.8 Hz), we apply spectral balancing (Bensen et al., 2007), which broadens the band of the signal. The spectral balancing is achieved by dividing each spectral amplitude by a local mean. The mean is taken over all samples within a 0.12 Hz window. The spectral balancing mitigates the depletion of energy at the high end of the spectrum due to rupture effects (corner frequency) and propagation effects (attenuation), thus balancing the contribution of all spectral frequencies and equalizing it for the different earthquakes to enhance the stacking later on.

- Then, we autocorrelate the phase response on the Z component of each earthquake at each station and repeat the autocorrelation for all events. The autocorrelation of individual events at each station is stacked to suppress incoherent features and enhance coherent features (e.g. Pham and Tkalcic, 2017, and references therein). When applying seismic interferometry to responses from distant seismicity, the stacking also serves to suppress reflectivity from the lithosphere at the source. This is further discussed in the next section.

- The next steps of the processing is the removal of the delta pulse, a coherent and high amplitude pulse at t=0. Since a wide frequency band was used in the autocorrelations, a relatively narrow delta pulse is obtained, which is removed by muting the first second and applying a Hanning taper from 1 to 6 seconds. The lower frequencies, however, have limited information content on the receiver-side structure. They are subsequently removed with a high-pass filter with a cutoff frequency at 0.2 Hz.

- Then a static correction is applied to account for the varying heights of the stations above sea level.

- A one-dimensional surface-related multiple elimination scheme (Verschuur and Berkhout, 1997) is done. Therewith, multiples from horizontal interfaces are largely suppressed. In the migration it is assumed that there are only primary reflections. Hence, this step helps to clean out a part of the multiple reflections that otherwise would be migrated to spurious reflectivity.

We test the method using different sub-ensembles of our selected 64 events, as shown in Figure 2 and in the supplementary material (Figures S1 to S8). For each sub-ensemble, we produce four panels showing the a) basic amplitude retrieval (BAR), which corresponds to the stack of autocorrelated traces after spectral balancing; b) the delta pulse removal; c) multiple suppression; d) the same as c) for actual station distance.

The final image of the crust is then depth-migrated using a velocity model obtained from deep seismic refraction/wide-angle reflection profiling along the Alp01 profile (Bleibinhaus et al., 2004). This refraction profile provides an estimate of the P-waves velocities of the crust and uppermost mantle for the region between profile distances 140km and 300km (we show in Figure S10 the P- velocity model and how it compares to other models).

3 RESULTS

To avoid geometrical distortions when imaging with a strong reflection-transmission signal, the interface should be planar and continuous over at least 20 km, which corresponds to the first Fresnel volume in teleseismic waves considering an average Moho depth of 40 km and frequencies of ~0.8Hz. Shorter, irregularly dipping and separated interface sections may appear as consistent reflectors despite their irregular or segmented nature (similar to the effects observed in active reflection seismics, e.g. Clauser, 2018). Within the lithosphere, the Moho is the strongest first order interface and we will consider the signal generated only by the Moho for our interpretation to avoid interpreting artifacts. We show in the supplementary text and figures S1 to S8 how the results of the application of the GloPSI are sensitive to the choice of the pool of events used for imaging (both concerning the spatial distribution, the magnitude and a balanced number of events on the two sides of the profile). When a small number of sources is used, strong horizontal artifacts can be seen over the interferometric result. The origin of these artifacts are cross-terms between first arrivals and depth phases. In Ruigrok and Wapenaar (2012), only 17 global phases could be used and a few cross-terms remained visible after applying seismic interferometry. The cross-terms were suppressed by removing the average over the array, at the cost of also removing real features that are horizontal over a large part of the array. For EASI, many more global phases are available (64 instead of 17) and no average removal is applied. In Figure S8, we use a subset of 27 phases selected according to the epicentral location and magnitude. For this selection, we avoided to include clusters, referring to multiple events with epicentres located within 3 degrees in both distance and backazimuth. In each cluster, we included the event with the highest magnitude (listed in Table T1). We show that in this case the choice of the events delivers a stable and reliable interferometric image, little differing from the image retrieved by including all possible events (Figure 2).

Within the GloPSI images, we look for the blue-red-blue triplet (e.g. Ruigrok and Wapenaar, 2012) as marker of a positive impedance contrast (increasing velocity with depth). The Moho is imaged as a triplet signature with a red (positive) signal in the centre and the typical two side lobes of the wavelet creating such characteristic blue-red-blue feature. We computed the GloPSI response for 100 bootstrapped sets of events (for both cases of including 64 and 27 events). The results have been used to estimate the mean and standard deviation of the amplitudes associated with the images, and are shown in Figure 3 for the

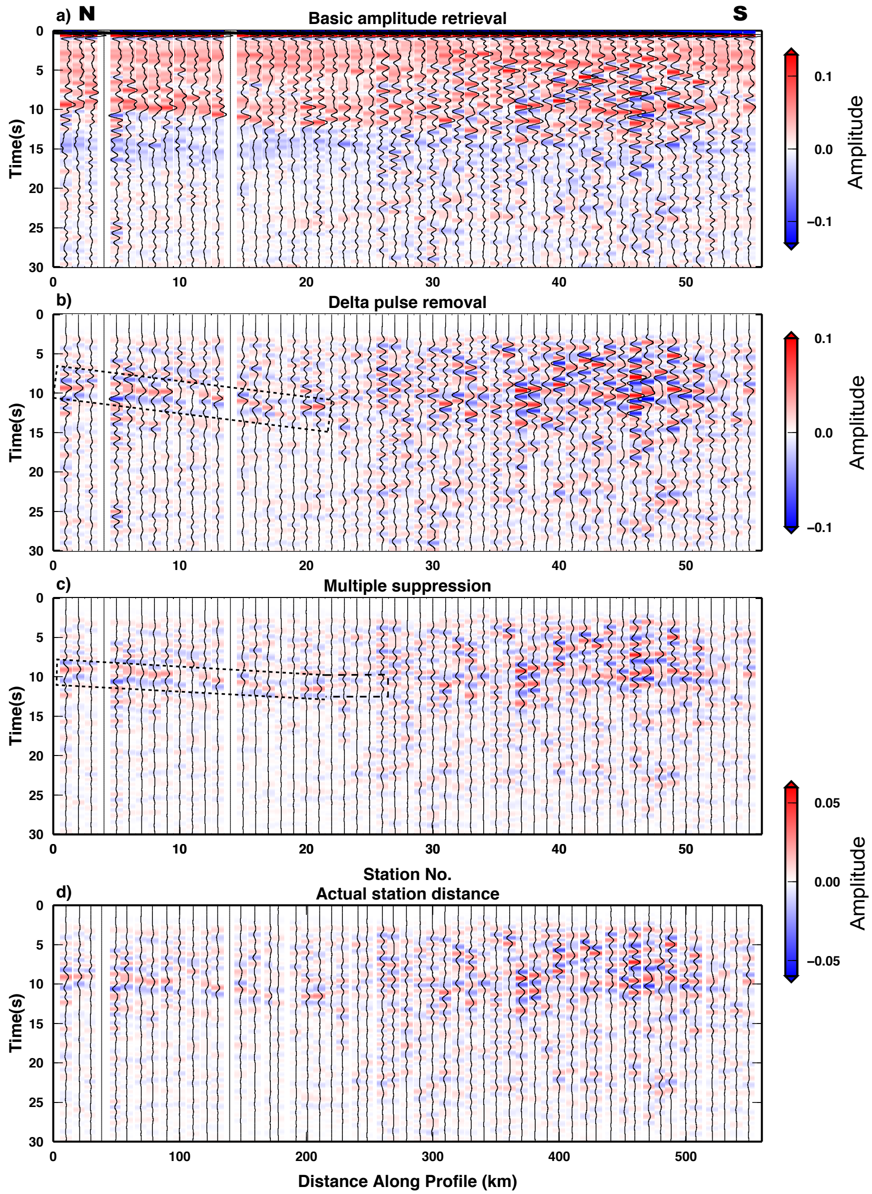

Figure 2. Steps of the GloPSI processing on the ensemble of 64 events listed in Table T1. (a) Basic amplitude retrieval, (b) delta pulse removal, (c) multiple correction and static correction, (d) amplitudes displayed according to the station distance along the north-south direction. Blue-red-blue triplet is outlined between dashed lines in panels b and c.

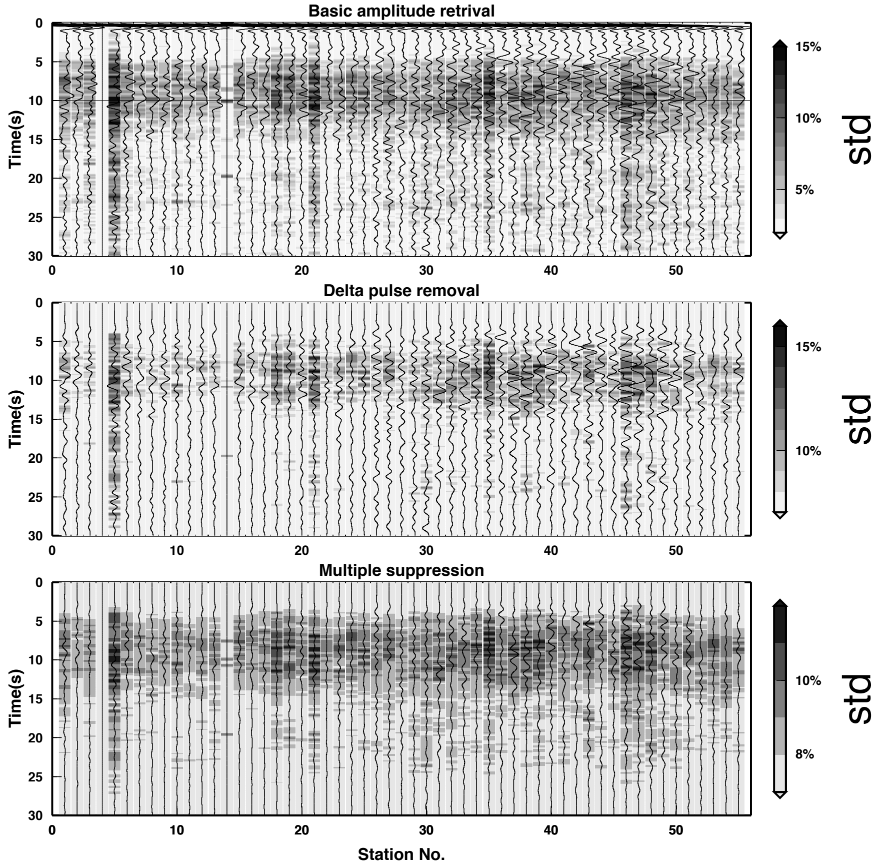

Figure 3. Standard deviation calculated over 100 samples generated by bootstrapping events ensembles by the pool of 64 events (Table T1). Mean wiggles are displayed on top of the std.

64 events and in Figure S9 for the 27 events. The three panels in both Figures (3 and S9) display the STD as percentage of the maximum amplitude of the relative panels in Figures 2 and S8. In both figures the northernmost 30 stations show smaller standard deviation values, meaning that the autocorrelated traces are more similar to each other for this part of the transect, while in the southern part of the transect the traces have larger variability.

Figure 4 shows the depth migrated GloPSI results along the EASI profile for (a) the subset of 27 teleseismic sources and (b) the entire dataset (64 teleseismic sources). The two migrated images are quite similar, despite the large difference in input. This gives confidence that especially receiver-side reflectivity is shown on these images and most of the cross-terms due to source-side reveberations (SSR) have been suppressed. Remnant SSR artifacts can be noticed by features that are stronger in Figure 4a than in Figure 4b and marked at depth between 65 and 85 km (area 1 and 2, Figure 4a). These features are disappearing in the northern part of the profile (area 1) and decreasing in amplitude in the southern part of the profile (area 2, Figure 4b). This shows that adding more phases with different SSRs, simply helps in unveiling the receiver-side structure.

Below the Alps (southern part of the profile, area 2 in Figure 4) not much difference can be noted between the two migrated images. Hence, also at larger depths, both images are already dominated by receiver-side reflectivity. Nevertheless, a part of the imaged amplitudes at larger depth is spurious. In a complex scattering environment like the Alps, there could e.g. be P-S conversion on steep reflectors that end up at the zero-offset response. With the underlying assumption that only P-wave reflectivity is retrieved, these conversions are then wrongly imaged. We decide to use the image obtained with 64 events (Figure 4b) and to focus our interpretation on the Moho topography in the northern part of the profile.

In the migrated image in Figure 4b, we pick the maximum amplitude (within the blue-red-blue triplet) in the 0-270 km section of the profile for the 64 events (Figure 4b). We then smooth this interface for a 50 km Fresnel zone for deriving the Moho topography (Figure 4c). In Figure 4c also marked is a poorly resolved section of the Moho at the southernmost end. The relatively strong amplitude signals in the crust are nearly identical for either 64 events (Figure 4b) or 27 events (Figure 4a) and, therefore, can only be attributed to reflectivity beneath the receiver array. Note that while these moderate to strong amplitude signals of relatively short length (up to 50km) above the Moho signal are rather common in GloPSI results (e.g. Ruigrok and Wapenaar, 2012) and while they are visible all along the EASI profile, beneath the Alps (from profile distance 300km to 520km) they dominate the image from the top of the crust to where we would expect the Moho based on previously published CSS data (Yan and Mechie, 1989). The difference in the image of these "crustal features" between profile distance 0km and 300km (Bohemian massif and northern Alpine foreland) and below the Eastern Alpine orogen, suggest the signals representing at least in parts internal crustal structure. Unfortunately, the 3D crustal structure of the Eastern Alps below 15 km depth is still poorly known (Behm et al., 2007; Lu et al., 2020; Qorbani et al., 2020), compared with the well-known crustal structures beneath the Central and Western Alps (e.g. Kissling et al., 2006) and with reference to the tectonic style and geologic evolution of the orogeny (e.g. Willingshofer et al., 2013; Rosenberg and Kissling, 2013, and references therein). However, we can expect a rather complex crustal structure beneath the Eastern Alps, in particular, regarding the lower crust and the crustal root (Handy et al., 2015). Furthermore, while extrapolations of the Moho topography along the EASI transect across the plate boundary beneath the Alps from CSS profiling (e.g. Brückl et al., 2007) and from RF (Hetényi et al., 2018) differ substantially, they agree in the great complexity of the crust-mantle transition zone. The suggested structural complexity of the internal Alpine crustal structure correlates very well with our GloPSI results. If the European Moho continued to descend smoothly toward south beyond profile distance 270 km and if it was overlain by a simple crustal structure of laterally continuous layers, the crust would just increase in thickness and exhibit smooth lateral velocity variations. GloPSI would show this distinct change across the northern Alpine front.

4 DISCUSSION

The Moho GloPSI results obtained in this study are documented as a migrated image in Figure 4c and compared with published information about the Moho along the EASI transect in Figure 5. In the GloPSI image we notice a clear divide between two domains along the EASI transect. The northern part of the profile (0 to 270 km, possibly 300 km distance along profile, Figure 4b), is characterized by low amplitude reflectors within the crust and one pronounced feature (both in amplitude and length)

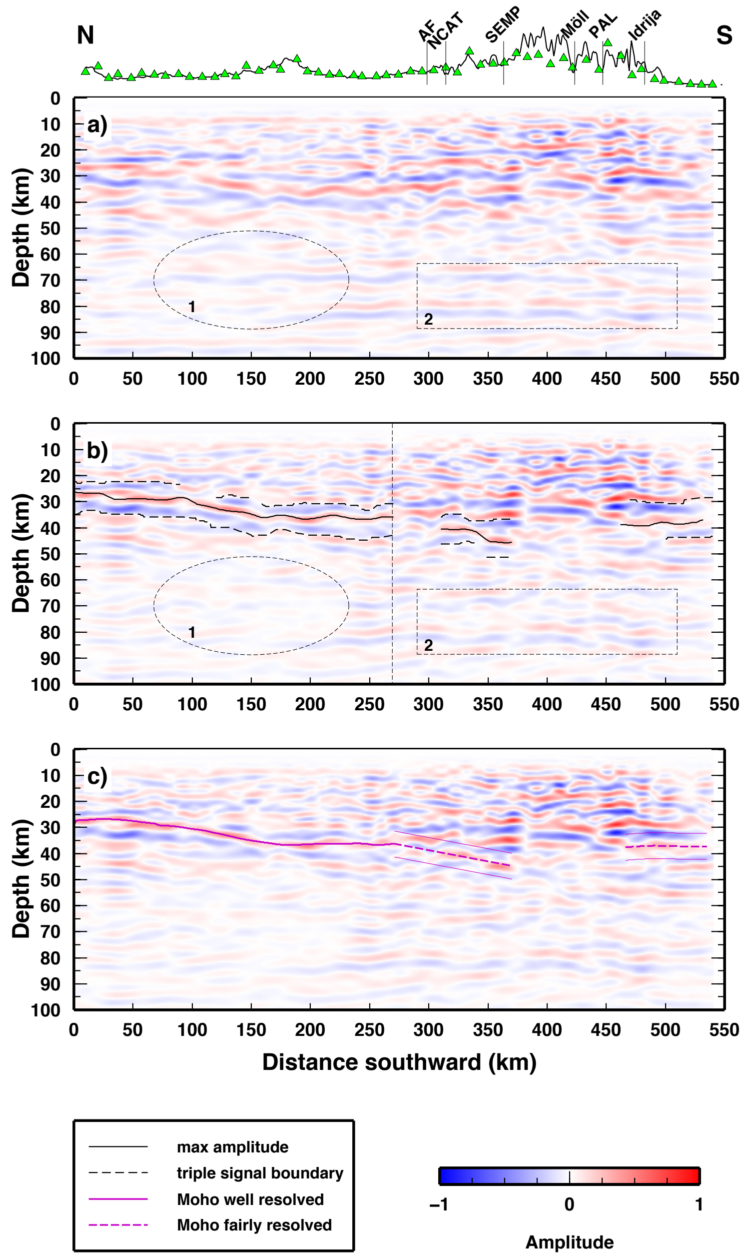

Figure 4. Reflectivity images of the crust and upper mantle along EASI; in the background the interpolated figure (bilinear interpolation), in which blue-red-blue triplet marks the presence of a positive interface (i.e. an increasing impedance contrast with depth). a) Depth migrated GloPSI image generated by using 27 events. b) Depth migrated GloPSI image generated by using 64 events, black solid line marks the maximum amplitude within the blue-red-blue triplet, black dashed line marks the upper and lower boundary of the triplet; features 1 and 2 are described in the text. c) background same as (b), solid and dashed purple line show the picked Moho depths reported in Table T2.

that can univocally be related to the Moho interface above the uppermost mantle lithosphere that is nearly transparent. The southern part of the profile instead (south of about 300 km), is characterized by high amplitude reflectivity within the whole crust. The observed alternation of positive and negative phases may suggest the presence of a complex velocity structure with several interfaces of strong velocity discontinuities. In Figure 5 we included the information from several CSS studies (5b and 5d) and from RF (5c) studies. In particular, the CSS profiles analysed by Hrubcova and Geissler (2009) and by Yan and Mechie (1989), are crossing the EASI profile at 110 and 375 km respectively, and they provide two reference points for the Moho depth (stars in Figure 5b, 5d). We compare our image also with the refraction seismic model by Brückl et al. (2007) and the Moho depths from the study of Spada et al. (2013), which combined the published CSS profile results with well-resolved Moho depths based on PmP wide-angle reflections (from Behm, 2006). The strength of our new results lies in the continuous assessment of the lateral variation of the Moho interface and thus well documents the Moho topography in the northern part of the profile (Figure 5a). Our results suggest that of the previously published information for the profile distance 50 to 100 km, the shallower PmP Moho (Spada et al. (2013) based on Behm (2006)) is probably more accurate than the CSS profile model (Brückl et al., 2007) (see depth-enhanced Figure 5d), while in the profile distance 100 to 270km the opposite is true with the refraction profile model showing the subhorizontal Moho at about 34 km. Hrubcová et al. (2005) documented a layer of anomalously high-velocity of 7.0 km/s regionally varying in thickness up to 12 km above the Moho. This layer, if taken into account in the depth migration of the GloPSI image, would shift the retrieved Moho towards shallower depth, and closer to the Moho of Spada et al. (2013). Our results beyond profile distance 270 km (latest at 300 km) are difficult to interpret, anyways all available CSS information calls for a distinct increase in the dip of the Moho exactly beneath the Northern Alpine Front at 300km profile distance. For further comparison, in Figure 5c, we plot on top of our GloPSI image the punctual measurements of the Moho depth obtained by depth migrated S-RF (Bianchi et al., 2014), and by the ZK analysis (Zhu and Kanamori, 2000) of P-RF (Bianchi et al., 2015) that were retrieved from stations located within 20 km distance from EASI. We also compare our image with the Moho topography obtained by Hetényi et al. (2018) with pre-stack migration (PSM) of P-RF along EASI. Our results and the results of this latter, show good agreement from the northern end of the EASI profile to 150 km distance. In this part of the profile, the signals both from RF and GloPSI are clear (Figure 5c) and we can, therefore, infer the presence of one strong impedance contrast across the Moho. In combination with the results shown in Figure 5b we conclude the Moho is well imaged univocally by all methods in this northernmost section. Between 150 and 270 km profile distance we notice the divergence between our GloPSI Moho image and results presented by Hetényi et al. (2018) (Figure 5c). The laterally varying differences in depth of the Moho might be caused either by errors in the crustal velocity estimates used for depth migration, or by the presence of several crustal or mantle features that deviate from being horizontally layered. Considering the Moho results of the refraction seismic profile Alp01 (Brückl et al., 2007) that are rather well resolved in this region, the latter seems unlikely. In the southernmost part of the profile (400 to 550 km distance), the steep northward dip of the Adriatic Moho interpreted by PSM imaging (Figure 5c) is not seen by our results. As stated previously, the GloPSI method is suitable for identifying sub-horizontal to gently-dipping interfaces. In this part of the profile (440 to 550 km distance), the Moho estimates from single station analysis have been derived by depth migrated SRF (Bianchi et al., 2014). The low frequency of the used S-wave is the reason for the large errors associated with these depth estimates, and from such analysis it would not be possible to separate the contribution of more than one impedance contrast at depth. Moreover, the two different depths inferred from the same station (circled in Figure 5c) are suggesting the presence of several impedance contrasts in the crust for this section of the profile. As last comparison, previous RF studies on crustal structures (Bianchi and Bokelmann, 2014), located anisotropy at the mid-lower crust, extending from the SEMP fault southward (feature 3 in Figure 5c). From the GloPSI, in this area (SEMP and southward, lower-crust) we see a high reflectivity pattern. The co-located high reflectivity (from GloPSI) and anisotropy (from RF), are possibly due to the same physical reasons (e.g. layering or imbrication), which contribute to fading the Moho signal beneath the Alps. In summary, the reliably resolved GloPSI results nicely complement the published results along the EASI transect derived from CSS and RF studies (Figure 5). As discussed above, the three seismic methods exhibit different strength and limitations but they are all particularly sensitive to the first-order velocity discontinuity that represents the crust-mantle boundary. The correspondence of the Moho depth obtained by the 3 different seismic methods in the northernmost 150km of the profile suggests a crust and a Moho in this part of the northern Alpine foreland that correlates well with the models for the continental crust proposed by Mueller (1977) and Musacchio et al. (1998) and with the crustal models published for the northern foreland further west (e.g. Ye et al., 1995). Our GloPSI results and those published from CSS studies continue to correspond well further south beneath the Molasse basin (to profile distance 270 km and possibly 300 km) to the northern limits of the Eastern Alps. In this section of the transect, we note that the RF results show significant lateral variations in depth and also differences between the two RF studies. Since the study of Hetényi et al. (2018) is confined to the temporary stations of the EASI profile and the study of Bianchi et al. (2015), is punctually sampling wider region including permanent stations, these differences possibly reflect lateral velocity variations in the crust beneath the Molasse basin and further south in the northernmost Alps. Moreover, Hetényi et al. (2018) uses the regional Vp and Vs model from Molinari and Morelli (2011) for migrating the Moho Ps conversions. We instead, use a transect specific Vp model (Brückl et al., 2007), which is much more detailed and reliable for the EASI transect.

In accordance with findings in the Western and Central Alps (e.g. Schmid and Kissling, 2000), our GloPSI results document a complex crustal structure beneath the Eastern Alps. While this complexity prevents us from further interpreting any signals south of profile distance 300 km, a number of studies have proposed models of the deep structure beneath the Alps. As Figures 5b and 5c show, these models differ greatly in the estimated Moho topography across the plate boundary. With the exception of the CSS longitudinal profile by Yan and Mechie (1989), all studies suffer from limitations of the method or the data set, or both, to reliably resolve the crustal structure and Moho topography in this most interesting region. In the Eastern Alps, the number of CSS profiles and experiments for academic reasons is limited, and the restoration of subsurface geometries yields to ambiguous results due to the 3D charachteristics of the orogenic root. Obviously, with respect to the complex velocity structure in the crust and the strongly dipping Moho interfaces that characterize the Alpine orogen, true 3D seismic methods such as, f.e., local earthquake tomography, are needed to reliably assess the 3D velocity field of the crust, subsequently allowing to correct for crustal structure when imaging the Moho topography with RF or other methods across the plate boundary.

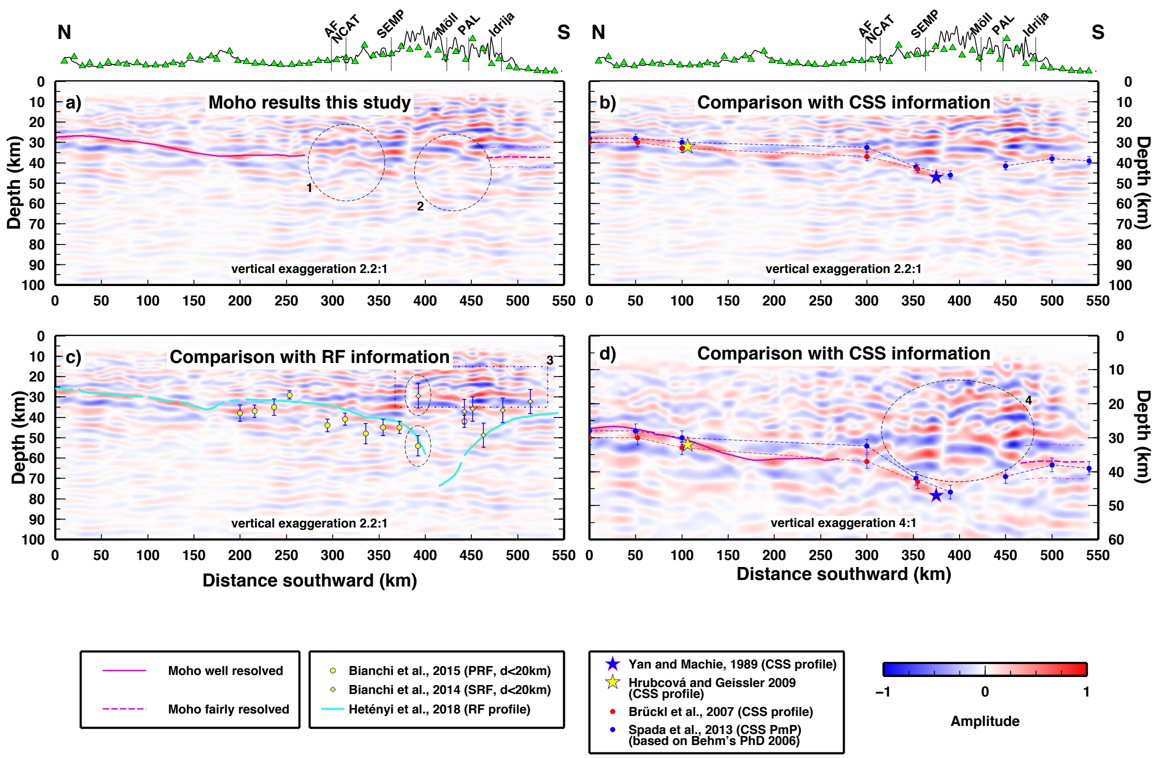

Figure 5. Reflectivity images of the crust and upper mantle along EASI; in the background the interpolated figure as in Figure 4b. a) Moho topography beneath the northern Alpine foreland and the Alps as detailed by results of this study. The subhorizontal and gently dipping Moho is well imaged by our global phase interferometry but the typical Moho signal disappears beneath the central parts of the Eastern Alps (features 1 and 2). b) Comparison with CSS information documenting the generally good correlation between our new Moho results and previous information on crustal thickness outside the Alps. c) Comparison with RF information where we evidence the co-location of the high reflectivity of crust and the detected anisotropic layer (feature 3). d) Comparison with CSS information in an enlarged version allows highlighting more detail and it reveals a nearly perfect correspondence with the PmP model (Behm, 2006; Spada et al., 2013) in the north and an equally good correspondence with the refraction seismic model (Brückl et al., 2007)) in the southern part of the foreland. The strong reverberation directly beneath the Alps (4) documents the complex internal crustal structure of the orogen.

5 Conclusions

We applied global phase interferometry to data collected by the passive seismic deployment EASI, which crosscuts the Eastern Alps along a 550 km long north-south profile. Inferring the crustal thickness and the nature of the Moho below the Alpine crests has been challenging in the last decades, and has led to different and often opposing interpretations. In this work, we have the opportunity to review and compare previous information on Moho depth, aside producing a new image of the crust. From north to south we can follow the different responses of the crust to the different imaging techniques (GloPSI, CSS and RF). In the northernmost part of the profile we obtain consistent depth estimates, which suggest a very simple crustal structure and a high impedance contrast at the Moho. Between 100 and 270 km along profile, we observe diverging Moho depth estimates, which might be due to an anomalously high-velocity lowermost crustal layer, known to exist below parts of the Bohemian massif, or/and to lateral variations or local topography of the Moho interface. Between profile distance 270 and 300 km, the GloPSI does not deliver a clear image of the Moho, due to the southern dip of the European plate. The segment of the profile between 300 and 550 km is the most controversial, and the one hosting the long debated and inaccessible crust-mantle boundary. The application of this technique did not constrain the Moho topography immediately beneath the Eastern Alps, but did image the complex lower crustal structure. To univocally image the crust-mantle transition below the Eastern Alps, we further need to address this area by integrating and combining several seismic methods and by increasing the seismic station density.

Acknowledgements. We thank J. Plomerová and G. Hetényi for their major contribution to the realization, deployment and maintenance of the EASI seismic transect. IB thanks G. Bokelmann, F. Fuchs, P. Kolinský and the other members of the IMG Vienna, for the support given to the realization and logistics of the Viennese contribution to the EASI project. We thank the Alparray-EASI Field Team: Jaroslava Plomerová, Helena Munzarová, Ludek Vecsey, Petr Jedlicka, Josef Kotek, Irene Bianchi, Maria-Theresia Apoloner, Florian Fuchs, Patrick Ott, Ehsan Qorbani, Katalin Gribovszki, Peter Kolinsky, Peter Jordakiev, Hans Huber, Stefano Solarino, Aladino Govoni, Simone Salimbeni, Lucia Margheriti, Adriano Cavaliere, John Clinton, Roman Racine, Sacha Barman, Robert Tanner, Pascal Graf, Laura Ermert, Anne Obermann, Stefan Hiemer, Meysam Rezaeifar, Edith Korger, Ludwig Auer, Korbinian Sager, György Hetényi, Irene Molinari, Marcus Herrmann, Saulé Zukauskaité, Paula Koelemeijer, Sascha Winterberg. We thank F. Bleibinhaus for providing his P-wave velocity model of the ALP2002-01 profile, used here for the depth migration. IB acknowledges the support of the Austrian Science Fund (FWF) Project J 4314-N29. We thank the SPP 4DMB project for making public the generalized tectonic map of the Alps (http://www.spp-mountainbuilding.de), which we used in Figure 1.

6 Data availability

The data is distributed through EIDA (European Integrated Data Archive), ETH node. Tha entire dataset is open since October 2018. The EASI network code is XT.

Author contributions. I.B., E.R., A.O. and E.K. contributed to the design and implementation of the research, to the analysis of the results and to the writing of the manuscript.

Competing interests. I.B. is part of the Topical Editor pool of this Journal.

References

Adams, R. and Randall, D.: Observed Triplication of PKP, Nature, 200, 744–745, 1963.

AlpArray Working Group: AlpArray Seismic Network (2014): Eastern Alpine Seismic Investigation (EASI) - AlpArray Complimentary Experiment, http://data.datacite.org/10.12686/alparray/xt_2014, 2014.

Amante, C. and Eakins, B.: NETOPO1 1 Arc-Minute Global Relief Model: Procedures, Data Sources and Analysis. NOAA Technical Memorandum NESDIS NGDC-24., doi:10.7289/V5C8276M, 2009.

Behm, M.: Accuracy and resolution of a 3D seismic model of the Eastern Alps, Ph.D. thesis, The school of the thesis, Vienna University of Technology, phD Thesis, 2006.

Behm, M., Brückl, E., Chwatal, W., and Thybo, H.: Application of stacking and inversion techniques to three-dimensional wide-angle reflection and refraction seismic data of the Eastern Alps, Geophysical Journal International, 170, 275–298, https://doi.org/10.1111/j.1365-246X.2007.03393.x, 2007.

Bensen, G. D., Ritzwoller, M. H., Barmin, M. P., Levshin, A. L., Lin, F., Moschetti, M. P., Shapiro, N. M., and Yang, Y.: Processing seismic ambient noise data to obtain reliable broad-band surface wave dispersion measurements, Geophysical Journal International, 169, 1239–1260, https://doi.org/10.1111/j.1365-246X.2007.03374.x, 2007.

Bianchi, I. and Bokelmann, G.: Seismic signature of the Alpine indentation, evidence from the Eastern Alps, Journal of Geodynamics, 82, 69 – 77, https://doi.org/https://doi.org/10.1016/j.jog.2014.07.005, sI : Geodynamics of the Mediterranean, 2014.

Bianchi, I., Miller, M. S., and Bokelmann, G.: Insights on the upper mantle beneath the Eastern Alps, Earth and Planetary Science Letters, 403, 199 – 209, https://doi.org/https://doi.org/10.1016/j.epsl.2014.06.051, 2014.

Bianchi, I., Behm, M., Rumpfhuber, E. M., and Bokelmann, G.: A New Seismic Data Set on the Depth of the Moho in the Alps, Pure and Applied Geophysics, 172, 295 – 308, https://doi.org/10.1007/s00024-014-0953-1, 2015.

Bigi, G., Cosentino, D., Parotto, M., Sartori, R., and Scandone, P.: Structural model of Italy, 1:500.000, Quaderni de La Ricerca Scientifica, C.N.R., 114, 1990.

Bleibinhaus, F. and Brückl, E.: Wide-angle observations of ALP 2002 shots on the TRANSALP profile: Linking the two DSS projects, Tectonophysics, 414, 71 – 78, https://doi.org/https://doi.org/10.1016/j.tecto.2005.10.027, 2006.

Bleibinhaus, F. and Gebrande, H.: Crustal structure of the Eastern Alps along the TRANSALP profile from wide-angle seismic tomography, Tectonophysics, 414, 51 – 69, https://doi.org/https://doi.org/10.1016/j.tecto.2005.10.028, tRANSALP, 2006.

Bleibinhaus, F., Brückl, E., Gosar, A., Grad, M., Hegedus, E., Hrubcová, P., Keller, R., Šumanovac, F., Yliniemi, J., and Group, A. . W.: Alp 2002 Experiment-2D Raytracing modelling and seismic tomography of selected profiles, 32nd International Geological Congress-Florence, 2004.

Blundell, D., Freeman, R., and Mueller, S.: A Continent Revealed, the European Geotraverse, Cambridge University Press, New York, 1992.

Bousquet, R., Schmid, S., Zeilinger, G., Oberh ansli, R., Rosenberg, C., Molli, G., Robert, C., Wiederkehr, M., and Rossi, P.: Tectonic framework of the Alps., 2012.

Brückl, E., Bodoky, T., Hegedüs, E., Hrubcová, P., Gosar, A., Grad, M., Guterch, A., Hajnal, Z., Keller, G., Špičák, A., Sumanovac, F., Thybo, H., Weber, F., Aric, K., Behm, M., Bleibinhaus, F., Broz, M., Chwatal, W., Gebrande, H., Grassl, H., Harder, S., Hock, S., Höck, V., Joergensen, P., Kohlbeck, F., Miller, K., Rumpfhuber, E., Schmid, C., Schmöller, R., Snelson, C., Tiira, T., Tomek, Č., Ullrich, C., Wilde-Piórko, M., and Yliniemi, J.: ALP 2002 seismic experiment, Studia Geophysica et Geodaetica, 47, 671–679, https://doi.org/10.1023/A:1024780022139, 2003.

Brückl, E., Bleibinhaus, F., Gosar, A., Grad, M., Guterch, A., Hrubcová, P., Keller, G. R., Majdaáski, M., umanovac, F., Tiira, T., Yliniemi, J., Hegedűs, E., and Thybo, H.: Crustal structure due to collisional and escape tectonics in the Eastern Alps region based on profiles Alp01 and Alp02 from the ALP 2002 seismic experiment, Journal of Geophysical Research: Solid Earth, 112, https://doi.org/10.1029/2006JB004687, 2007.

Claerbout, J. F.: Synthesis of a layered medium from its acoustic transmission response, Geophysics, 33, 264–269, https://doi.org/10.1190/1.1439927, 1968.

Clauser, C.: Seismik, pp. 5–232, Springer Berlin Heidelberg, Berlin, Heidelberg, https://doi.org/10.1007/978-3-662-55310-7_2, 2018.

Diehl, T., Husen, S., Kissling, E., and Deichmann, N.: High-resolution 3-D P-wave model of the Alpine crust, Geophysical Journal International, 179, 1133–1147, https://doi.org/10.1111/j.1365-246X.2009.04331.x, 2009.

Fantoni, R., DellaVedova, B., Guistiniani, M., Nicolich, R., Barbieri, C., DelBen, A., Finetti, I., and Castellarin, A.: Deep seismic profiles through the Venetian and Adriatic foreland (Northern Italy), Mem. Sci. Geol., 54, 131–134, 2003.

Frank, J. G., Ruigrok, E. N., and Wapenaar, K.: Shear wave seismic interferometry for lithospheric imaging: Application to southern Mexico, Journal of Geophysical Research: Solid Earth, 119, 5713–5726, https://doi.org/10.1002/2013JB010692, 2014.

Froitzheim, N., Schmid, S., and Frey, M.: Mesozoic paleogeography and the timing of eclogite-facies metamorphism in the Alps: a working hypothesis, Eclogae Geologicae Helvetiae, 89, 81, 1996.

Grad, M., Bruckl, E., Majdanski, M., Behm, M., Guterch, A., 2000, C., and Groups, A. . W.: Crustal structure of the Eastern Alps and their foreland: Seismic model beneath the CEL10/Alp04 profile and tectonic implications, Geophysical Journal International, 177, 279–295, https://doi.org/10.1111/j.1365-246X.2008.04074.x, 2009.

Guterch, A., Grad, M., Špičak, A., Bruckl, E., Heedus, E., Keller, G., and Thybo, H.: An overview of recent seismic refraction experiments in Central Europe, Studia Geophyica et Geodaetica, 47, 651–657, https://doi.org/https://doi.org/10.1023/A:1024775921231, 2004.

Handy, M. R., M. Schmid, S., Bousquet, R., Kissling, E., and Bernoulli, D.: Reconciling plate-tectonic reconstructions of Alpine Tethys with the geological–geophysical record of spreading and subduction in the Alps, Earth-Science Reviews, 102, 121 – 158, https://doi.org/https://doi.org/10.1016/j.earscirev.2010.06.002, 2010.

Handy, M. R., Ustaszewski, K., and Kissling, E.: Reconstructing the Alps–Carpathians–Dinarides as a key to understanding switches in subduction polarity, slab gaps and surface motion, International Journal of Earth Sciences, 104, https://doi.org/10.1007/s00531-014-1060-3, 2015.

Hetényi, G., Plomerová, J., Bianchi, I., Kampfová Exnerová, H., Bokelmann, G., Handy, M. R., and Babuška, V.: From mountain summits to roots: Crustal structure of the Eastern Alps and Bohemian Massif along longitude 13.3°E, Tectonophysics, 744, 239 – 255, https://doi.org/https://doi.org/10.1016/j.tecto.2018.07.001, 2018.

Holliger, K. and Kissling, E.: Ray theoretical depth migration— methodology and application to deep seismic-reflection data across the Eastern and Southern Swiss-Alps, Eclogae Geol. Helv.,, 84, 369–402, 1991.

Hrubcova, P. and Geissler, W. H.: The crust-mantle transition and the Moho beneath the Vogtland/West Bohemian region in the light of different seismic methods, Studia Geophysica et Geodaetica, 53, 275 – 294, https://doi.org/10.1007/s11200-009-0018-6, 2009.

Hrubcová, P., Środa, P., Špičák, A., Guterch, A., Grad, M., Keller, G. R., Brueckl, E., and Thybo, H.: Crustal and uppermost mantle structure of the Bohemian Massif based on CELEBRATION 2000 data, Journal of Geophysical Research: Solid Earth, 110, https://doi.org/10.1029/2004JB003080, 2005.

Kissling, E., Schmid, S. M., Lippitsch, R., Ansorge, J., and Fügenschuh, B.: Lithosphere structure and tectonic evolution of the Alpine arc: new evidence from high-resolution teleseismic tomography, Geological Society, London, Memoirs, 32, 129–145, https://doi.org/10.1144/GSL.MEM.2006.032.01.08, https://mem.lyellcollection.org/content/32/1/129, 2006.

Kummerow, J., Kind, R., Oncken, O., Giese, P., Ryberg, T., Wylegalla, K., and Scherbaum, F.: A natural and controlled source seismic profile through the Eastern Alps: TRANSALP, Earth and Planetary Science Letters, 225, 115 – 129, https://doi.org/https://doi.org/10.1016/j.epsl.2004.05.040, 2004.

Lu, Y., Stehly, L., Brossier, R., Paul, A., and AlpArray Working Group: Imaging Alpine crust using ambient noise wave-equation tomography, Geophysical Journal International, 222, 69–85, https://doi.org/10.1093/gji/ggaa145, 2020.

Molinari, I. and Morelli, A.: EPcrust: a reference crustal model for the European Plate, Geophysical Journal International, 185, 352–364, https://doi.org/10.1111/j.1365-246X.2011.04940.x, 2011.

Molinari, I., Obermann, A., Kissling, E., Hetényi, G., and Boschi, L.: 3D crustal structure of the Eastern Alpine region from ambient noise tomography, Results in Geophysical Sciences, 1-4, 100 006, https://doi.org/https://doi.org/10.1016/j.ringps.2020.100006, 2020.

Mueller, S.: A New Model of the Continental Crust, pp. 289–317, American Geophysical Union (AGU), https://doi.org/10.1029/GM020p0289, 1977.

Musacchio, G., Zappone, A., Cassinis, R., and Scarascia, S.: Petrographic interpretation of a complex seismic crust–mantle transition in the central-eastern Alps, Tectonophysics, 294, 75 – 88, https://doi.org/https://doi.org/10.1016/S0040-1951(98)00094-8, 1998.

Neubauer, F., Gensler, J., and Handler, R.: The Eastern Alps: Result of a two-stage collision process, Mitt. Österr. Geol. Ges., pp. 117–134, 2000.

Nishitsuji, Y., Ruigrok, E., Gomez, M., Wapenaar, K., and Draganov, D.: Reflection imaging of aseismic zones of the Nazca slab by global-phase seismic interferometry, Interpretation, 4, SJ1–SJ16, https://doi.org/10.1190/INT-2015-0225.1, 2016.

NOAA National Geophysical Data Center: NOAA National Geophysical Data Center. 2009: ETOPO1 1 Arc-Minute Global Relief Model. NOAA National Centers for Environmental Information, doi:10.7289/V5C8276M, Accessed: 2019.

Pfiffner, O., Lehner, P., Heitzmann, P., Mueller, S., and Steck, A. e.: Deep Structure of the Swiss Alps., Birkhaeuser, Basel, 1997.

Pham, T. and Tkalcic, H.: On the feasibility and use of teleseismic P wave coda autocorrelation for mapping shallow seismic discontinuities, Journal of Geophysical Research: Solid Earth, 122, 3776–3791, https://doi.org/10.1002/2017JB013975, 2017.

Qorbani, E., Zigone, D., Handy, M. R., Bokelmann, G., and working group, A.-E.: Crustal structures beneath the Eastern and Southern Alps from ambient noise tomography, Solid Earth, 11, 1947–1968, https://doi.org/10.5194/se-11-1947-2020, 2020.

Rosenberg, C. L. and Kissling, E.: Three-dimensional insight into Central-Alpine collision: Lower-plate or upper-plate indentation?, Geology, 41, 1219–1222, https://doi.org/10.1130/G34584.1, 2013.

Rosenberg, C. L., Schneider, S., Scharf, A., Bertrand, A., Hammerschmidt, K., Rabaute, A., and Brun, J.-P.: Relating collisional kinematics to exhumation processes in the Eastern Alps, Earth-Science Reviews, 176, 311 – 344, https://doi.org/https://doi.org/10.1016/j.earscirev.2017.10.013, 2018.

Roure, F., Heitzmann, P., and Polino, R. e.: EDeep Structure of the Alps, 1990.

Ruigrok, E. and Wapenaar, K.: Global-phase seismic interferometry unveils P-wave reflectivity below the Himalayas and Tibet, Geophysical Research Letters, 39, https://doi.org/10.1029/2012GL051672, 2012.

Ruigrok, E., Campman, X., Draganov, D., and Wapenaar, K.: High-resolution lithospheric imaging with seismic interferometry, Geophysical Journal International, 183, 339–357, https://doi.org/10.1111/j.1365-246X.2010.04724.x, 2010.

Sadeghi-Bagherabadi, A., Vuan, A., Aoudia, A., Parolai, S., and the AlpArray and AlpArray-Swath-D W. Group: High-resolution crustal S-wave velocity model and Moho geometry beneath the Southeastern Alps: new insights from the SWATH-D experiment, Frontiers in Earth Science, submitted.

Scarascia, S. and Cassinis, R.: Crustal structures in the central-eastern Alpine sector: A revision of the available DSS data, Tectonophysics, 271, 157 – 188, https://doi.org/https://doi.org/10.1016/S0040-1951(96)00206-5, 1997.

Schmid, S., Fügenschuh, B., Kissling, E., and Schuster, R.: Tectonic Map and overall architecture of the Alpine orogen, Eclogae Geologicae Helvetiae, 97 (1), 93–117, 2004.

Schmid, S., Bernoulli, D., Fügenschuh, B., Matenco, L., Schefer, S., Schuster, R., and Ustaszewski, K.: The Alpine-Carpathian-Dinaridic orogenic system: correlation and evolution of tectonic units, Swiss Journal of Geosciences, 101, 139–183, 2008.

Schmid, S. M. and Kissling, E.: The arc of the western Alps in the light of geophysical data on deep crustal structure, Tectonics, 19, 62–85, https://doi.org/10.1029/1999TC900057, 2000.

Schuster, G. T.: Theory of daylight/interferometric imaging: Tutorial, 63rd Conference Technical Exhibition, EAGE, extended Abstracts, 2001.

Snieder, R.: Extracting the Green's function from the correlation of coda waves: A derivation based on stationary phase, Phys. Rev., 69, 046610, 2004.

Spada, M., Bianchi, I., Kissling, E., Agostinetti, N. P., and Wiemer, S.: Combining controlled-source seismology and receiver function information to derive 3-D Moho topography for Italy, Geophysical Journal International, 194, 1050–1068, https://doi.org/10.1093/gji/ggt148, 2013.

Sun, W. and Kennett, B. L. N.: Receiver structure from teleseisms: Autocorrelation and cross correlation, Geophysical Research Letters, 43, 6234–6242, https://doi.org/10.1002/2016GL069564, 2016.

Tauzin, B., Pham, T.-S., and Tkalčić, H.: Receiver functions from seismic interferometry: a practical guide, Geophysical Journal International, 217, 1–24, https://doi.org/10.1093/gji/ggz002, 2019.

TRANSALP Working Group, Gebrande, H., Lüschen, E., Bopp, M., Bleibinhaus, F., Lammerer, B., Oncken, O., Stiller, M., Kummerow, J., Kind, R., Millahn, K., Grassl, H., Neubauer, F., Bertelli, L., Borrini, D., Fantoni, R., Pessina, C., Sella, M., Castellarin, A., Nicolich, R., Mazzotti, A., and Bernabini, M.: First deep seismic reflection images of the Eastern Alps reveal giant crustal wedges and transcrustal ramps, Geophysical Research Letters, 29, 92–1–92–4, https://doi.org/10.1029/2002GL014911, 2002.

Van Ijsseldijk, J., Ruigrok, E., Verdel, A., and Weemstra, C.: Shallow crustal imaging using distant, high-magnitude earthquakes, Geophysical Journal International, 219, 1082–1091, https://doi.org/10.1093/gji/ggz343, 2019.

Verschuur, D. J. and Berkhout, A. J.: Estimation of multiple scattering by iterative inversion; Part II, Practical aspects and examples, Geophysics, 62, 1596–1611, https://doi.org/10.1190/1.1444262, 1997.

Waldhauser, F., Lippitsch, R., Kissling, E., and Ansorge, J.: High-resolution teleseismic tomography of upper-mantle structure using an a priori three-dimensional crustal model, Geophysical Journal International, 150, 403–414, https://doi.org/10.1046/j.1365-246X.2002.01690.x, 2002.

Wapenaar, K.: Synthesis of an inhomogeneous medium from its acoustic transmission response, GEOPHYSICS, 68, 1756–1759, https://doi.org/10.1190/1.1620649, 2003.

Willingshofer, E., Sokoutis, D., Luth, S., Beekman, F., and Cloetingh, S.: Subduction and deformation of the continental lithosphere in response to plate and crust-mantle coupling, Geology, 41, 1239–1242, https://doi.org/10.1130/G34815.1, 2013.

Yan, Q. Z. and Mechie, J.: A fine structural section through the crust and lower lithosphere along the axial region of the Alps, Geophysical Journal International, 98, 465–488, https://doi.org/10.1111/j.1365-246X.1989.tb02284.x, 1989.

Ye, S., Ansorge, J., Kissling, E., and Mueller, S.: Crustal structure beneath the eastern Swiss Alps derived from seismic refraction data, Tectonophysics, 242, 199 – 221, https://doi.org/https://doi.org/10.1016/0040-1951(94)00209-R, 1995.

Zhu, L. and Kanamori, H.: Moho depth variation in southern California from teleseismic receiver functions, Journal of Geophysical Research: Solid Earth, 105, 2969–2980, https://doi.org/10.1029/1999JB900322, 2000.